# Ultra-Wide Swath SAR Imaging with Continuous PRF Variation

Nicolas Gebert, German Aerospace Center (DLR), Microwaves and Radar Institute, Wessling, Germany
Gerhard Krieger, German Aerospace Center (DLR), Microwaves and Radar Institute, Wessling, Germany

## Abstract

Innovative multi-channel synthetic aperture radar (SAR) concepts enable high-resolution wide-swath imaging, but the antenna length typically restricts the achievable swath width. This limitation can be overcome by a novel technique which is based on a single azimuth channel but operates the system with a continuously varied pulse repetition frequency (PRF) by this allowing in principle for arbitrary wide swaths. This paper introduces the basic principles and discusses design constraints for such a PRF variation. Further, a systematic performance analysis of an L-band reflector antenna system is carried out with focus on the sensitivity versus different input parameters.

## 1. Introduction

SAR is a well-established technique for remote sensing of the Earth. Unfortunately, a system-inherent limitation precludes state-of-the-art SAR with only a single transmit and receive channel from detailed imagery with continuous global coverage, as it is requested by future monitoring missions. This can be overcome by innovative SAR systems with multiple receive channels, which collect additional samples for each transmitted pulse, by this enabling high-resolution wide-swath imaging [2], [3].

For multiple receivers arranged in along-track direction, this directly translates into an increased effective sampling rate which enables an improved geometric resolution (cf. Fig. 1). Equivalently, the transmit PRF can be reduced while keeping the resolution constant. This enlarges the reception window between subsequent pulses and thus allows for a wider swath. Depending on the chosen PRF, a certain azimuth antenna length is imposed that (a) ensures illumination of the Doppler spectrum matched to the sampling rate and (b) avoids spatial sample positions deviating too strongly from uniform distribution [2], [3]. Regarding multiple receiver elements arranged in elevation dimension, beamforming allows for implementing one or more sharp pencil beams of high gain in a time dependent way such that only signals from the desired direction are received. This is of special interest in reflector antenna based systems (cf. Fig. 1, right), as beam steering requires at each instance of time only the combination of a small number of feed elements [4], [5].

The aforementioned concepts enable swath widths of 100 km, but imaging of larger swaths in stripmap mode fails. Basically, this is due to the blind ranges that occur when transmit and receive events coincide, hence blocking possible reception. This means the interpulse period PRI –i.e. the inverse PRF– defines the maximum continuous reception time and thus limits the swath in stripmap mode. On the other hand, the antenna length limits the minimum possible PRF, finally restricting the swath extension. A possible solution is given by the operation of multi-channel systems in burst modes. A system design example with a 400 km swath –allowing for a weekly imaging of the complete

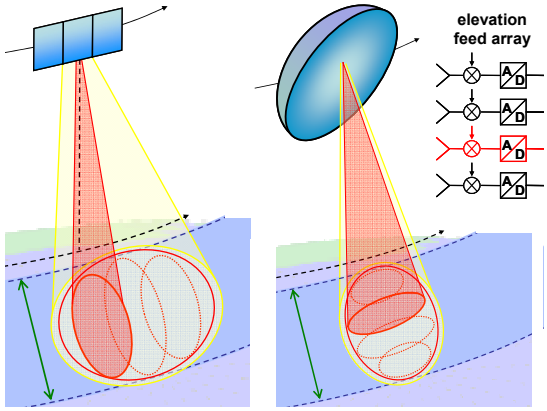


Fig. 1 Innovative SAR systems based on planar azimuth array (left) and reflector antenna with elevation feed array (right) [1].

Earth– and a geometric resolution of 5 m was shown in [4] and [6]. This is paid for by inconveniences linked with burst modes such as a performance depending on the target position and increased hardware cost to effectuate the necessary beam steering operations. Consequently, a novel approach based on the continuous variation of the PRF technique will be analyzed in the following. This method for the mapping of arbitrary wide swaths was first proposed in [7] and represents an attractive solution for ultra-wide swath imaging which does not even require multiple azimuth apertures.

## 2. Continuous PRF Variation

Conventional system operation relies on a constant $PRF_0$. Considering the timing, this entails discrete blind ranges as illustrated in Fig. 2 (red color). In contrast, continuous variation of the interval between transmitted pulses –equivalent to continuously varying the PRF– steadily shifts the corresponding blind range (cf. Fig. 2, green). As a result, the formerly discrete blind ranges disappear; they are now “distributed” according to the applied span of PRF values. In the end, continuous coverage is achieved at the cost of partial blockage, i.e. a loss of some pulses for every target. In consequence, the swath width is no longer limited by the applied PRF thus enabling unprecedented wide coverage. Effectively, this PRF variation results in a non-uniform sampling of the synthetic aperture. In consequence, ad-

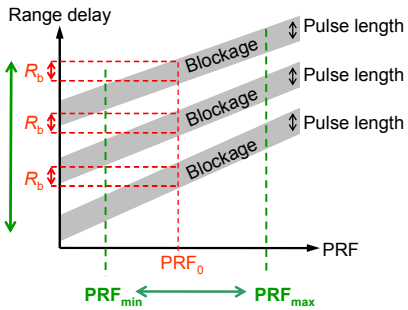


Fig. 2 Blockage of reception due to transmit events (gray) for range delay vs. PRF. A constant $PRF_0$ causes blind regions $R_b$ (red). In contrast, continuous variation from $PRF_{min}$ to $PRF_{max}$ steadily shifts the blockage region, by this avoiding specific blind ranges (green).

ditional processing is required which has to account for the respectively applied PRF variation. In the following, a simple interpolation is applied to re-sample the signal to a regular azimuth grid.

Basically, an arbitrary variation of the interpulse interval is possible. Although a random variation offers some interesting features, the present paper concentrates on a linear variation of the PRI ("sweep"). In this case, the sweep period $T_{sw}$ and ΔPRF, which defines the variation from $PRF_{min}$ to $PRF_{max}$, have to be defined and will be derived in the following.

Firstly, it makes sense to illuminate every target by the complete ΔPRF. Hence, the interval length $T_{sw}$ for one full PRF sweep should not exceed the synthetic aperture. Assuming a required Doppler bandwidth $B_D$, (1) quantifies the upper bound of the sweep period:

$$T_{sw} \le \frac{R_{0,\min} \cdot \lambda}{2 \cdot v_s \cdot v_g} \cdot B_D \,, \qquad (1)$$

with wavelength λ, sensor velocity $v_s$, beam footprint velocity $v_g$, and minimum slant range $R_{0,min}$. Note that the following considerations also apply for shorter sweep periods, as long as granulation effects are avoided by a sufficiently large number of pulses per $T_{sw}$. Very short periods deserve separate discussion, which is beyond the scope of this paper.

Secondly, ΔPRF has to be large enough to span the blockage region and additionally leave the target exposed long enough to ensure the required Doppler bandwidth. Assume a period of $M$ samples, a pulse length τ, and a slant range $R_0$ specified by its 2-way delay $t_0=2 \cdot R_0/c_0$, with $c_0$ the speed of light. The number of emitted pulses between transmission and reception of a specific pulse are denoted by $p_{tr}$. If the PRF varies only little over $p_{tr}$, these "traveling pulses" can be approximated by (2), where ⌊·⌋ indicates the floored integer.

$$p_{tr} = \left\lfloor \frac{2 \cdot R_0}{c_0} \cdot \mathrm{PRF} \right\rfloor \qquad (2)$$

Consider a pulse to be fully lost as soon as it is no longer received completely. Then, as the PRF variation is monotonic, each pulse sequence of constant $p_{tr}$ contains only a single gap. This blockage starts with the pulse at index $m_0$ (obtained for '-') and ends at index $m_1$, which is defined by '+'.

$$m_{0,1} = \left( \frac{p_{tr} \cdot \mathrm{PRF}_{min}^{-1} - t_0 \mp \tau}{p_{tr} \cdot \left( \mathrm{PRF}_{min}^{-1} - \mathrm{PRF}_{max}^{-1} \right)} \right) \cdot (M-1) + \frac{3}{2} - \frac{p_{tr}}{2} \qquad (3)$$

The number of blocked samples $|m_b|$ can be quantified by (4), where $PRF_m$ defines the geometric PRF mean and $dc_m$ the associated duty cycle.

$$\frac{|m_b|}{M-1} = \frac{2 \cdot \tau}{p_{tr}} \cdot \frac{\mathrm{PRF}_{min} \cdot \mathrm{PRF}_{max}}{\mathrm{PRF}_{max} - \mathrm{PRF}_{min}} = \frac{2 \cdot dc_m \cdot \mathrm{PRF}_m}{p_{tr} \cdot \Delta\mathrm{PRF}} \qquad (4)$$

For a PRF variation such that $p_{tr}$ changes, (3) and (4) can be applied repeatedly to determine the amount of lost pulses. If the mean PRF and pulse length are fixed, (4) finally imposes a minimum ΔPRF for a maximum tolerable loss. As (4) gives the worst case for full pulse loss, considering also partially received pulses will reduce the loss and relax the restrictions.

Regarding an upper bound for ΔPRF, there is no limit imposed by the principle of PRF variation. However, the best achievable ratio between reception and blockage is already obtained when the "reception window" is maximized but only a single gap is encountered. Then, there is no benefit in further increasing ΔPRF. Transferred to (4), a single gap means a constant $p_{tr}$. In a simplified approach not taking into account $PRF_{min}$ and $PRF_{max}$ but only their offset, $\Delta PRF_{max}$ can be approximated by the maximum PRF span over which $p_{tr}$ remains constant in far range (cf. (2)).

One recognizes that both blockage and reception depend on slant range. For the applied linear variation of the interpulse period, this unavoidably entails a non-constant system performance. To achieve a constant ratio between lost and received pulses independent of slant range, a sophisticated variation scheme tailored to the specific timing would be required. Such optimization strategies are currently under investigation.

## 3. Example system

Consider a reflector antenna system similar to Tandem-L/DESDynI [1] as specified in Table I. Firstly, the system parameters are inserted in (1). For a processed Doppler bandwidth of 900 Hz and a mean PRF of 1600 Hz, one obtains a maximum sweep period of ~2900 pulses. In the following, this slow variation will be compared to a variation five times faster, i.e. a period

| Parameter | Symbol | Value |
|---|---|---|
| Orbit height | $h_s$ | 760 km |
| Carrier wavelength | $\lambda$ | 0.2384 m |
| Coverage (off-nadir angle) | $\Theta_r$ | 27.2° – 42.9° |
| Swath width on ground | $W_g$ | ≥ 350 km |
| Slant range | $R_0$ | 868 – 1097 km |
| Sensor velocity | $v_s$ | 7473 m/s |
| Beam velocity | $v_g$ | 6631 - 6664m/s |
| Minimum PRF | $PRF_{min}$ | 1535 Hz |
| Maximum PRF | $PRF_{max}$ | 1665 Hz |
| Mean PRF | PRF | ~1600 Hz |
| Reflector antenna diameter | $l_{az}$ | 15 m |
| Transmit pulse length | $\tau$ | 10 µs, 20 µs |
| Processed Doppler band- | $B_D$ | 900 Hz |
| Chirp bandwidth | $B_{rg}$ | 20 MHz |

TABLE I. SYSTEM PARAMETERS.

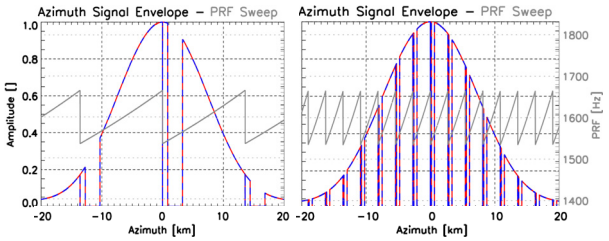


Fig. 3 Azimuth signal envelope (red/blue) overlaid by the applied PRF variation (gray). Slow variation over 2900 pulses (left) and fast variation with a period of 580 pulses (right). $R_0$=868 km, τ=40 µs.

of 580 pulses. Next, the PRF span leading in far range to an increment of $p_{tr}$ by 1, is derived from (2). One obtains a ΔPRF of 130 Hz.

For the exemplary (near) slant range $R_0$ of 868 km, the azimuth signal envelope after range compression (blue/red) and the PRF variation (gray) vs. azimuth are depicted in Fig. 3. It shows the results for a completely lost pulse of 40 µs. For the slow sweep, long continuous regions change with rather long gaps, while the fast sweep entails many but rather short gaps. In average, the amount of lost pulses is the same for both sweeps.

In addition to a complete pulse loss, partially received pulses can be range compressed. This translates into a reduced azimuth amplitude according to the received portion of the chirp bandwidth.

## 4 Performance Analysis

This section analyzes the azimuth performance of a 2D point target signal for both a complete as well as a partial pulse loss during the eclipses. To recover the non-equally sampled azimuth grid, interpolation is applied after range compression. Finally, for azimuth focusing a Doppler band of 900 Hz is considered.

Firstly, snapshots of the impulse response for different target positions and sweep periods are shown, to demonstrate the impact of the PRF variation. Fig. 4 gives the azimuth response for ΔPRF=130 Hz and $R_0$=868 km, considering a partially lost pulse of 20 µs. One observes strong variations with the target position for a long period (top) while hardly any variation is encountered for the fast sweep (bottom). Additionally, grating lobes pop up for the fast variation. These grating lobes are introduced in the SAR impulse response by the periodicity of the PRF variation. The along-track separation $x_{off,g}$ of the grating lobes is directly dependent on the period $T_{sw}$ and can be quantified as:

$$x_{\text{off,g}} = \frac{R_0 \cdot \lambda}{2 \cdot v_s \cdot T_{sw}} \tag{5}$$

Secondly, the key performance figures are systematically analyzed in dependency on different shifts of the PRF ramp normalized to the sweep period. This is equivalent to different target positions, "normalized" to the distance defined by a full period. Fig. 5 summarizes for a fast and a slow sweep rate, respectively, the results for the following parameters:

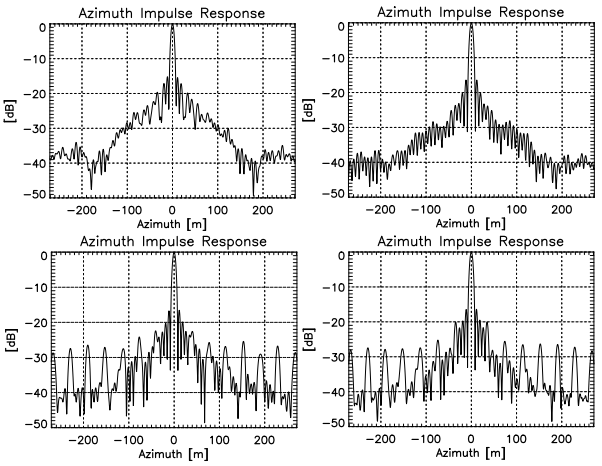


Fig. 4 Azimuth impulse response for a period of 2900 (top) and 580 pulses (bottom). Left and right show two different target positions shifted by 1/3 of the period, i.e. by 193 and 966 pulses, respectively.

- *Geometric resolution in azimuth* $\delta_{az}$, defined as the 3 dB width of the impulse response function.
- *Integrated side lobe ratio* ISLR, defined as the energy within the main lobe and the first (two-sided) side lobe related to the energy outside this region.
- *Azimuth ambiguity-to-signal ratio* AASR, determined for the respective energies.
- Normalized *signal peak power*.

Simulations are performed for different pulse lengths of 10 µs and 20 µs, respectively, as well as for a complete ("Full") and partial ("Part.") loss of the pulse during blockage. The results are coded by different colors and line-styles according to the legend. Finally, the results obtained for system operation with a constant PRF are included as a reference ("Ref.") or used for normalization of the peak power (cf. Fig. 5).

One observes that different performance parameters show different sensitivity against the variations. AASR and resolution show only moderate dependency on both pulse length and target position. The signal peak power varies straightforward with the pulse length, but only little with target position. Finally, the ISLR shows a strong dependency on τ. Further, it is very sensitive against changes of the target position for long sweep periods, but varies only little for the fast sweep.

Quantitatively, the fast variation leads to better results in terms of a worst case criterion. In this case, the relevant Tandem-L scenario (τ=20 µs, consideration of the partial range spectral support) yields a resolution better than 7 m. AASR and ISLR are below -26.5 dB and -10.5 dB, respectively, and a moderate peak power loss of ~0.5 dB is encountered. To sum up, the dramatically increased swath width of 350 km is mainly bought by a degradation of the ISLR.

In general, one can conclude that the performance is dominated by size and position of the gap in the signal. The larger the gap, the worse the performance, as can be well observed for the reduced sensitivity against the eclipses if the partly received pulses are also con-

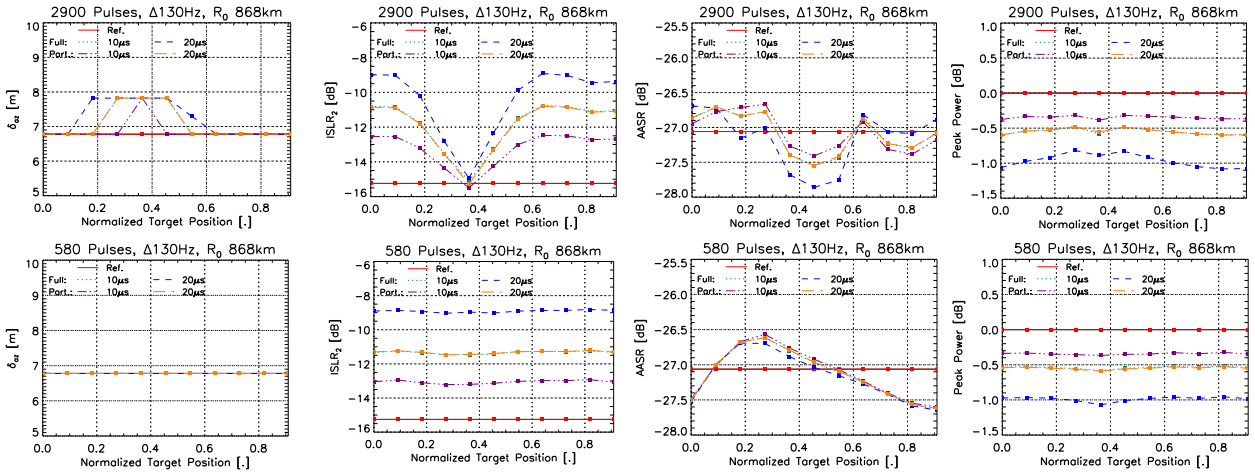


Fig. 5 Geometric resolution in azimuth (left), ISLR (middle left), AASR (middle right) and normalized peak power (right) vs. normalized target position for a sweep period of 2900 (top) and 580 pulses (bottom). $R_0$=868 km, ΔPRF=130 Hz, τ = 10 μs and 20 μs.

sidered. Further, longer periods entail a larger variation with target position, as the gap position within the signal might vary strongly. In contrast, a shorter period clearly decreases the sensitivity of the performance against target position, but also worsens the average performance. In addition, the issue of grating lobes has to be kept in mind for short sweep periods.

## 6 Summary and Discussion

The paper introduces a novel concept for imaging ultra-wide swaths by employing a continuous PRF variation. This allows for eliminating blind ranges at the cost of periodic losses in the azimuth raw data signal. In a first step, system design constraints are discussed and investigated analytically. Next, a systematic comparison of the system performance with respect to different input parameters is given. As a result, the performance varies depending on the target position and the pulse length τ which governs the mean duty cycle. In general, the variations are the stronger, the longer the period of the sweep is and the bigger the pulse length τ and the associated gap in the signal are. In the considered order of magnitude, the sweep range ΔPRF has only a minor impact. Further, according to the sweep period, grating lobes will occur. For long periods, these lobes are folded back and directly modify the main lobe of the impulse response. Last but not least, a fast sweep period clearly reduces the variations against target position and a nearly constant performance can be obtained. Unfortunately, this might be at the cost of a worsened average performance. In summary, the performance is clearly dominated by size and position of the gap; its shape is of minor importance. Nevertheless, for the investigated system scenario the PRF variation has successfully demonstrated to enable ultra-wide swaths of 350 km with good performance, despite only a simple interpolation technique was used. Further performance improvement is expected from advanced processing strategies. Such optimized concepts which do not solely recover the irregular sampling grid but additionally aim at coping with the gaps in the data are currently under investigation.

It should be noted that a straightforward burst mode processing with multiple looks –as e.g. in ScanSAR– would allow getting rid of the effects induced by the periodic gaps. Of course such an approach is only suitable if the unavoidably associated coarse azimuth resolution can be tolerated, as e.g. for interferometric applications where one directly benefits from multiple azimuth looks.

Furthermore, very fast as well as random variation schemes appear promising and deserve further study. Finally, the "visual" impact of periodic gaps in a SAR image will be evaluated soon with spaceborne data acquired by TerraSAR-X.

## References


[1] G. Krieger et al., "The Tandem-L Mission Proposal: Monitoring Earth's Dynamics with High Resolution SAR Interferometry," *Proc. IEEE Radar Conference (RadarCon),* Pasadena, CA, USA, May 2009.

[2] N. Gebert, G. Krieger, and A. Moreira, "Digital Beamforming on Receive: Techniques and Optimization Strategies for High-Resolution Wide-Swath SAR Imaging", *IEEE Trans. Aerosp. Electron. Syst.*, vol. 45 (2), pp. 564-592, Apr. 2009.

[3] N. Gebert, "Multi-Channel Azimuth Processing for High-Resolution Wide-Swath SAR Imaging", Dissertation Universität Karlsruhe (TH), *DLR-Forschungsbericht 2009-13*, ISSN 1434-8454, Wessling, Germany, Jun.. 2009.

[4] G. Krieger, N. Gebert, M. Younis, F. Bordoni, A. Patyuchenko, and A. Moreira, "Advanced Concepts for Ultra-Wide-Swath SAR Imaging", *Proc. of European Conference on Synthetic Aperture Radar* (*EUSAR*), Friedrichshafen, Germany, Jun. 2008.

[5] M. Younis; F. Bordoni, N. Gebert, and G. Krieger, "Smart Multichannel Radar Techniques for Spaceborne Remote Sensing", *Proc. of the IEEE International Geoscience and Remote Sensing Symposium (IGARSS)*, Boston, MA, USA, Jul. 2008.

[6] N. Gebert, G. Krieger, and A. Moreira, "Multichannel Azimuth Processing in ScanSAR and TOPS Mode Operation," *IEEE Trans. on Geosc. Remote Sens.*, accepted for publication in 2010.

[7] G. Krieger, N. Gebert, M. Younis, and A. Moreira, Advanced Synthetic Aperture Radar Based on Digital Beamforming and Waveform Diversity. *Proc. of the IEEE Radar Conference (RadarCon)*, Rome, Italy, May 2008.